JACC: BASIC TO TRANSLATIONAL SCIENCE VOL. 7, NO. 7, 2022


ORIGINAL RESEARCH - PRECLINICAL

# PTP1B Inhibition Improves Mitochondrial Dynamics to Alleviate Calcific Aortic Valve Disease Via Regulating OPA1 Homeostasis

Feng Liu, MD, Jinyong Chen, MD, Wangxing Hu, MD, PhD, Chenyang Gao, MD, PhD, Zhiru Zeng, MD, PhD, Si Cheng, MD, Kaixiang Yu, MD, PhD, Yi Qian, MD, Dilin Xu, MD, Gangjie Zhu, MD, Jing Zhao, MS, Xianbao Liu, MD, PhD, Jian'an Wang, MD, PhD

## VISUAL ABSTRACT

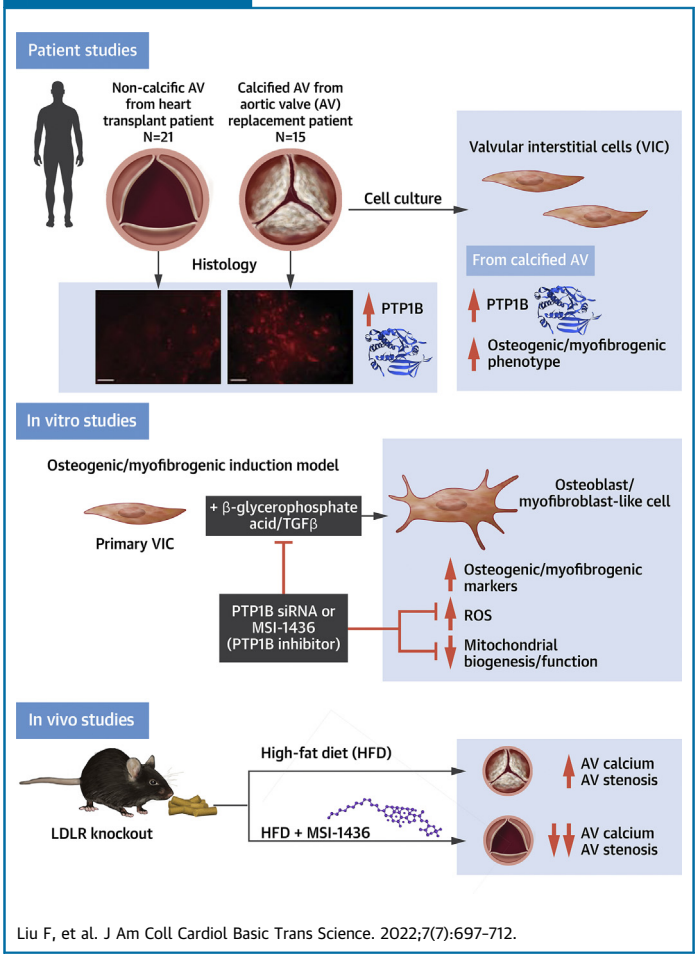


Liu F, et al. J Am Coll Cardiol Basic Trans Science. 2022;7(7):697–712.

## HIGHLIGHTS

- **Increased PTP1B was observed in the human calcified aortic valve leaflets and VIC osteogenesis, which indicated a novel association of PTP1B with aortic valve calcification.**
- **MSI-1436, a specific pharmacological PTP1B inhibitor, attenuated osteogenic and myofibrogenic differentiation of VICs, which coincided with preventing aortic valve fibrocalcific disease in a diet-induced mouse model of CAVD.**
- **Treatment of CAVD with PTP1B inhibitor mitigated the disorder of aortic jet velocity and mean gradient in vivo.**
- **PTP1B inhibition preserved the mitochondrial biogenesis and function in VIC osteogenesis via regulating OPA1 homeostasis.**

ISSN 2452-302X https://doi.org/10.1016/j.jacbts.2022.03.002

JACC: BASIC TO TRANSLATIONAL SCIENCE VOL. 7, NO. 7, 2022
JULY 2022:697–712

**ABBREVIATIONS AND ACRONYMS**

**β-GA** = β-glycerophosphate acid

**CAVD** = calcific aortic valve disease

**HFD** = high-fat diet

**L-OPA1** = long form of OPA1

**OPA1** = optic atrophy 1

**PTP1B** = protein tyrosine phosphatase 1B

**S-OPA1** = short form of OPA1

**TGFβ** = transforming growth factor β

**VIC** = valvular interstitial cell

**SUMMARY**

There are currently no pharmacological therapies for calcific aortic valve disease (CAVD). Here, we evaluated the role of protein tyrosine phosphatase 1B (PTP1B) inhibition in CAVD. Up-regulation of PTP1B was critically involved in calcified human aortic valve, and PTP1B inhibition had beneficial effects in preventing fibrocalcific response in valvular interstitial cells and $LDLR^{-/-}$ mice. In addition, we reported a novel function of PTP1B in regulating mitochondrial homeostasis by interacting with the OPA1 isoform transition in valvular interstitial cell osteogenesis. Thus, these findings have identified PTP1B as a potential target for preventing aortic valve calcification in patients with CAVD. (J Am Coll Cardiol Basic Trans Science 2022;7:697–712)


Calcific aortic valve disease (CAVD) is a progressive disease that has been occurring with rapidly increasing morbidity because of the ageing of the population.[1] Although mortality is not increased when aortic valve stenosis is asymptomatic, the death rate at 2 years is more than 50% for patients with symptomatic disease unless transcatheter or surgical aortic valve replacement is performed promptly.[2,3] There are currently no pharmacotherapies to prevent or reverse the progression of CAVD. Mounting evidence has indicated that CAVD was an active and regulable pathological process in which the risk factors, such as hyperlipemia and hypertension, are similar to those of other cardiovascular diseases.[4,5] However, lipid-lowering therapy with simvastatin and ezetimibe did not prevent the development of CAVD.[6] Therefore, the pathogenesis and molecular mechanism of CAVD need to be further explored. In this complex environment, initiation and progression of the disease thus seemed to be multifactorial, because aspects of lipid accumulation, inflammation, platelet activation, extracellular matrix remodeling, cellular senescence, and biomechanical forces have all been implicated in disease development.[7-9] The cellular mechanism for CAVD involved valvular interstitial cells (VICs) differentiating to osteoblast- and myofibroblast-like cells, which led to the progressive calcification and fibrosis of aortic valve leaflets.[10]

Protein tyrosine phosphatase 1B (PTP1B), encoded by PTPN1, is one of the most important members of the PTP family. It is anchored to the membrane of the endoplasmic reticulum by a catalytic N-terminal domain on the cytosolic side.[11] PTP1B has gained much attention in recent years because of its ability to regulate the insulin and leptin pathways by dephosphorylating tyrosine residues.[12] PTP1B inhibitors were recently considered an attractive treatment for insulin resistance and associated metabolic disorders.[13] In recent years, emerging evidence has suggested that PTP1B was widely expressed in cardiovascular tissues and that its inhibition could potentially be beneficial in the context of heart failure, myocardial infarction, and sepsis.[14-16] In addition, the pharmacological inhibition or myeloid deficiency of PTP1B protected against atherosclerotic plaque formation in a mouse model of atherosclerosis,[17,18] which indicated that PTP1B might also participate in the development of cardiovascular calcification.

Increasing evidence pointed to the critical role of localized inflammation and concomitant oxidative stress in the initiation and propagation phases of CAVD.[19] Cytokines secreted from macrophages and T cells, such as tumor necrosis factor α, interleukin-1β, and transforming growth factor β (TGFβ), induced the transition of VICs into myofibroblasts and osteoblasts.[20,21] In isolated cultured VICs, TGFβ induced reactive oxygen species (ROS) production, subsequently leading to calcium nodule formation in a signaling cascade involving the P38/MAPK and MEK1/2/ERK1/2 pathways.[22] These findings were replicated by exogenous ROS application, which promoted VICs calcification by up-regulating myofibrogenic and

From the Department of Cardiology of The Second Affiliated Hospital, School of Medicine, Zhejiang University, Hangzhou, China; and the Key Laboratory of Cardiovascular Disease of Zhejiang Province, Hangzhou, China.
The authors attest they are in compliance with human studies committees and animal welfare regulations of the authors' institutions and Food and Drug Administration guidelines, including patient consent where appropriate. For more information, visit the Author Center.

Manuscript received January 13, 2022; revised manuscript received March 1, 2022, accepted March 1, 2022.

osteogenic gene expression, indicating that oxidative stress might precede the differentiation of VICs to an osteoblastic phenotype.[23] Importantly, ROS have also been implicated in human calcified aortic valve leaflets. In explanted valves from patients with aortic valve stenosis, superoxide and $H_2O_2$ levels were markedly increased near the calcified regions of the valves.[24] Evidence supports the important role of oxidative stress in the mineralization of VICs, but the molecular process whereby oxidative stress induces an osteogenic response in the aortic valve is still poorly defined. It was reported that endothelial PTP1B deletion might mediate cardioprotective effects in heart failure through a reduction in ROS generation and NADPH oxidase (NOX) 4 expression.[14] In addition, a lack of PTP1B in hepatocytes treated with TGFβ caused an altered ratio of NOX1/NOX4, which generated ROS as their primary function.[25] Furthermore, a reduction in intracellular accumulated ROS and elevation in mitochondrial transmembrane potential after PTP1B inhibition were observed in adipose tissue.[26] Above all, PTP1B plays an important role in modulating oxidative stress in multiple tissues via both ROS-generating and ROS-scavenging mechanisms, but its role in oxidative stress-induced cardiovascular calcification is unknown.

In the present study, we performed a detailed analysis of clinical samples from patients with CAVD in conjunction with in vitro calcification studies of VICs to verify the possible effects of PTP1B inhibition on aortic valve calcification and the underlying mechanism modulating the osteogenesis of VICs.

## METHODS

Expanded methods are available in the Supplemental Appendix.

**HUMAN AORTIC VALVE COLLECTION.** Human calcified aortic valves were obtained from patients with CAVD who underwent surgical aortic valve replacement, and noncalcified aortic valves that exhibited no thickening or calcium deposition by echocardiography were obtained from patients with heart transplantation and with aortic valve regurgitation who underwent surgical aortic valve replacement. Exclusion criteria included rheumatic valvular disease, congenital valvular disease, and infective endocarditis. All samples involving humans complied with the Declaration of Helsinki and were approved by The Second Affiliated Hospital, School of Medicine, Zhejiang University (No. 2014-159). Informed consent was acquired from every patient before surgery. The isolated valve leaflets were divided into RIPA lysis buffer for protein extraction, embedding medium for immunofluorescence, and collagenase lysis buffer for isolation of primary human VICs.

**CELL CULTURE AND TREATMENT.** Primary human VICs were isolated from aortic valve leaflets, and purity of cell preparation was performed as described previously.[27] The isolated cells were stained with interstitial cell marker (Vimentin) and endothelial cell marker (CD31) for VIC characterization. VICs isolated from normal aortic valves were used for subsequent experiments at passage 3-7. To induce osteogenic differentiation of VICs, 10 mmol/L β-glycerophosphate acid (β-GA), 10 nmol/L dexamethasone, and 0.25 mmol/L ascorbic acid (β-GA system) or 2 mmol/L $Na_2HPO_4$ were added to complete medium for 14 days. To induce myofibrogenic differentiation, VICs were incubated in medium with 10 ng/mL recombinant human TGFβ for 7 days. The PTP1B-specific inhibitor, MSI-1436 lactate, was dissolved in dimethyl sulfoxide (DMSO) and added to the medium at a concentration of 20 μmol/L according to the results of preliminary experiment.

**CELL TRANSFECTION.** VICs were transfected with small interfering RNA (siRNA) targeting human PTP1B (PTP1Bsi), YME1-like 1 ATPase (YME1L1si), OMA1, and a control vector using RNAiMAX incubation for 6 hours. VICs were infected with recombinant lentivirus expressing the short hairpin RNA (shRNA) of PTP1B (PTP1Bsh), human optic atrophy 1 variant 1 (OPA1v1), variant 7 (OPA1v7), variant 8 (OPA1v8), YME1L1, and empty control vector. The sequences of siRNA and shRNA were listed in Supplemental Table 1.

**ANIMAL EXPERIMENTS.** Male low-density lipoprotein receptor $(LDLR)^{-/-}$ mice (C57BL/6 background) age 6-8 weeks were housed in a pathogen-free, temperature-controlled environment under a 12:12-hour light-dark cycle and fed a normal chow or a high-fat diet (HFD) for 24 weeks to develop aortic valve calcification as described previously.[27] The mice were randomly allocated to 3 groups: 1) NC group; 2) HFD group; and 3) HFD and MSI-1436 treatment (HFD + MSI group). The saline with PTP1B inhibitor MSI-1436 lactate (10 mg/kg) or DMSO was injected intraperitoneally monthly as described previously.[17] At the end of the protocol, transthoracic echocardiography was performed. Then, the mice were sacrificed, and their blood and hearts were collected. All animal studies were approved by the Institutional Animal Research Committee of Zhejiang University (No. 2019-177) and complied with the Guide for the Care and Use of

Laboratory Animals published by the U.S. National Institutes of Health.

**HEMATOXYLIN AND EOSIN STAINING AND MASSON'S TRICHROME STAINING.** Hematoxylin and eosin (H&E) staining was performed to assess the thickness of aortic valve leaflets as described previously.[28] The images were acquired by a light microscope, and quantitative analysis of aortic valve leaflet thickness was performed as described previously.[28] Good-quality valve leaflet sections of each group were chosen, and leaflet thickness was measured using ImageJ. Masson's trichrome staining was performed to assess the fibrosis on aortic valve leaflets as described previously.[29] Good-quality valve leaflet sections of each group were chosen, and the fractional areas of collagen fibrosis components (blue) in the aortic valve region were measured using ImageJ software.

**ALIZARIN RED STAINING AND VON KOSSA STAINING.** For alizarin red staining, the 4% paraformaldehyde fixed cells were stained with alizarin red solution, and the stained cells were photographed and quantified with a spectrophotometer at 405 nm.

Von Kossa staining was performed to assess the mineralization in aortic valve leaflets described previously.[30] The calcium deposition in the aortic valve leaflets was observed by a light microscope. Good-quality valve leaflet sections of each group were chosen, and the fractional areas of calcium nodule components (black and brown) in the aortic valve region were measured using ImageJ. Exclusion criteria included the dense, fusiform dark black mass on the leaflet surface (melanocyte).

**STATISTICAL ANALYSIS.** Quantitative values were denoted as the mean ± SD and representative data were obtained from at least 3 independent experimental replicates. The normality of distribution was determined using Shapiro-Wilk test or Kolmogorov-Smirnov test. Statistical differences were determined by 2-tailed unpaired Student's *t*-test for 2 groups and 1-way analysis of variance for 3 or more groups followed by Tukey's post hoc test for multiple pairwise comparisons. For skewed distributions, Kruskal-Wallis test was used to determine significance for multiple pairwise comparisons. Qualitative values were presented as counts with percentages and compared using the chi-square test. Statistical analyses were performed via Prism and SPSS. A value of $P < 0.05$ was considered statistically significant.

## RESULTS

**PTP1B IS INCREASED IN CAVD AND THE OSTEOGENIC DIFFERENTIATION OF VICs.** To verify the pathological characteristics of the collected human aortic valve samples, we performed H&E, Masson's trichrome, and Von Kossa staining, and representative staining images showed that the aortic valves from CAVD exhibited significant thickening, fibrosis, and calcification compared with those from the normal control (**Figure 1A**). We next measured the expression of PTP1B in aortic valve leaflets from both the normal control and CAVD groups by immunofluorescence (**Figure 1B**). The percentage of PTP1B-positive cells was relatively high in the calcified valves compared with normal valves (**Figure 1C**). The clinical characteristics of the patients were reported in **Table 1**. To further confirm this result, we documented the expression of PTP1B in the tissue lysates of normal and calcified aortic valves by Western blot. We found that the relative protein level of PTP1B was increased by 1.8-fold in the mineralized aortic valves (**Figure 1D**). To further investigate whether the difference between the control and CAVD groups was related to the different expression of PTP1B in VICs, we measured the PTP1B protein level in isolated VICs from a subset of control and CAVD samples. Isolated human VICs were characterized by immunostaining of interstitial and endothelial cell markers (Supplemental Figure 1). We found that VICs at passage 3 from the calcified valves had 2.5-fold PTP1B protein level as those from normal valves (**Figure 1E**). Thus, we determined whether PTP1B was involved in the osteogenic and myofibrogenic differentiation of normal human VICs in vitro. As shown in **Figures 1F, 1G, and 1H**, PTP1B was significantly increased in the β-GA and TGFβ medium treatments of VICs, but not in the $Na_2HPO_4$ treatment. In addition, immunofluorescent examination of the aortic valves from $LDLR^{-/-}$ mice fed a normal chow and a high-fat diet showed higher expression of PTP1B in the aortic valve leaflets from the HFD group than from normal chow (**Figure 1I and 1J**). Overall, this prominent association with the differentiation of VICs and PTP1B might suggest a potential role for PTP1B in the regulation of CAVD progression.

**INHIBITION AND KNOCKDOWN OF PTP1B PREVENT VIC OSTEOGENESIS IN VITRO.** We next hypothesized that inhibiting PTP1B might contribute to preventing VICs from differentiating into an osteoblast-like phenotype. Treatment with PTP1B-specific inhibitor MSI-1436 at a concentration of 20 μmol/L according to the results of preliminary experiment significantly attenuated calcium nodule formation in VICs stained with alizarin red after an osteogenic medium treatment for 2 weeks (**Figures 2A and 2B**). In addition, PTP1B inhibition decreased the protein levels of osteogenic markers, including alkaline

**FIGURE 1 PTP1B Was Highly Expressed in the Calcified Aortic Valves and the Osteogenic Differentiation of VICs**

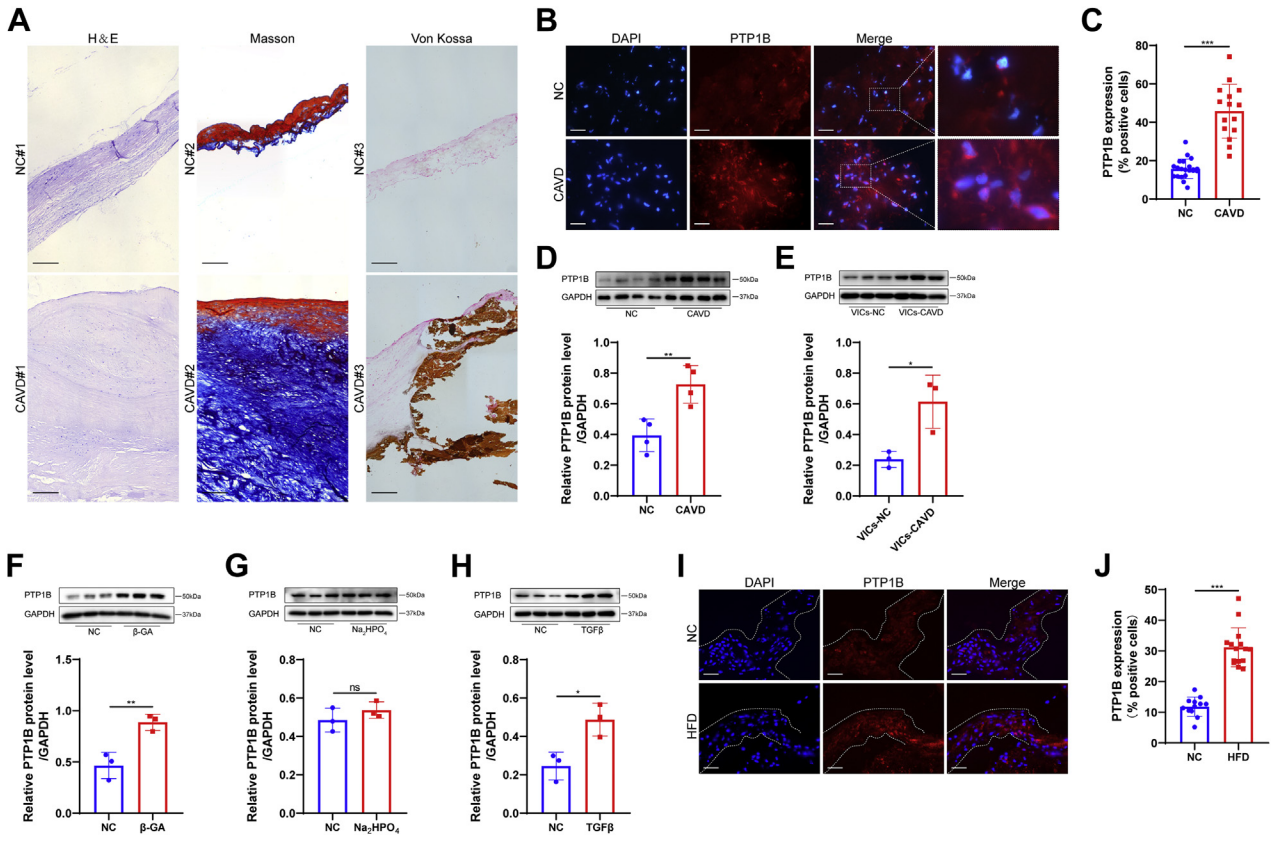


**(A)** Representative hematoxylin and eosin (H&E) staining, Masson's trichrome staining (Masson), and Von Kossa staining of the human aortic valve tissues from the normal control (NC) and calcific aortic valve disease (CAVD). **Scale bar:** 50 μm. **(B)** Representative PTP1B immunofluorescence staining images of human aortic valves from the NC and CAVD groups. **Scale bar:** 15 μm. **(C)** Quantitative analysis of the PTP1B-positive cells showed higher PTP1B expression in CAVD (n = 15) vs NC (n = 21). **(D)** The protein level of PTP1B in human aortic valve lysates was assessed by Western blot and quantified by normalizing to the glyceraldehyde-3-phosphate dehydrogenase (GAPDH) level (n = 4). **(E)** Quantitative analysis of the relative PTP1B protein levels in human valvular interstitial cells (VICs) at passage 3 isolated from normal valves (VICs-NC) and calcified aortic valves (VICs-CAVD; n = 3). **(F to H)** Relative PTP1B protein levels in VICs after treatment with β-glycerophosphoric acid (β-GA) **(F)**, $Na_2HPO_4$ **(G)**, and TGFβ **(H)** (n = 3). **(I)** Representative immunofluorescence staining images of PTP1B in aortic valves from the $LDLR^{-/-}$ mice fed a normal chow (NC) and a high-fat diet (HFD). **Scale bar:** 15 μm. **(J)** Quantitative data showed that the HFD group (n = 15) had significantly increased PTP1B expression in valve leaflets compared with that of a normal chow group (n = 12). Values are mean ± SD. The unpaired Student's *t*-test was performed. *$P < 0.05$; **$P < 0.01$; ***$P < 0.001$. DAPI = 4′,6-diamidino-2-phenylindole; ns = not significant.

phosphatase and RUNX2 in VIC osteogenesis (Figures 2C and 2D), which coincided with decreased alkaline phosphatase activity (Figure 2E). The identification of PTP1B knockdown in VICs by PTP1B siRNA and shRNA was shown in Supplemental Figures 2A and 2B. VICs transfected with PTP1B shRNA or the empty control vector lentivirus were cultured in osteogenic medium, and then we found that PTP1B knockdown decreased the mineralization of VICs (Figures 2F and 2G). Silencing PTP1B in VICs negated the increase in osteogenic markers (Figures 2H and 2I). Thus, our data verified the inhibitory effects of PTP1B inhibition and knockdown on the osteogenesis of VICs in vitro.

**MSI-1436 INHIBITS THE TGFβ-INDUCED OSTEOGENIC AND MYOFIBROGENIC DIFFERENTIATION OF VICs.** Because the activation of the myofibroblast-like phenotype by TGFβ was considered another critical step toward aortic valve stenosis, to further explore the effect of PTP1B in CAVD, we treated VICs with TGFβ (10 ng/mL) in the presence of MSI-1436 (20 μmol/L) or DMSO and assessed both the osteogenic and myofibrogenic markers. As expected, treatment with MSI-1436 reduced the expression of

**TABLE 1 Clinical Characteristics of Patients**

| | Normal Valve (n = 21) | Calcified Valve (n = 15) | *P* Valve |
|---|---|---|---|
| Age, y | 53 ± 12 | 61 ± 10 | 0.033 |
| Male | 15 (71.4) | 11 (73.3) | 0.900 |
| BMI, kg/m$^2$ | 23.2 ± 4.1 | 22.5 ± 2.9 | 0.560 |
| Smoking | 11 (52.4) | 7 (46.7) | 0.735 |
| Hypertension | 11 (52.4) | 6 (40) | 0.463 |
| Diabetes | 5 (23.8) | 1 (6.7) | 0.174 |
| Coronary heart disease | 5 (23.8) | 2 (13.3) | 0.434 |
| Statins | 3 (14.3) | 1 (6.7) | 0.473 |
| ACEI/ARBs | 7 (33.3) | 2 (13.3) | 0.172 |
| EF | 45.5 ± 17.4 | 57.5 ± 10.3 | 0.031 |
| Aortic valve area, cm$^2$ | – | 1.23 ± 0.74 | – |
| Aortic peak velocity, m/s | – | 4.12 ± 0.97 | – |
| Aortic max peak gradient, mm Hg | – | 71.5 ± 32.9 | – |
| Aortic mean peak gradient, mm Hg | – | 40.6 ± 20.5 | – |
| Total triglycerides, mmol/L | 1.20 ± 0.33 | 1.37 ± 0.62 | 0.829 |
| Total cholesterol, mmol/L | 4.51 ± 0.91 | 4.78 ± 1.16 | 0.469 |
| LDL, mmol/L | 2.36 ± 0.62 | 2.38 ± 0.61 | 0.921 |
| HDL, mmol/L | 1.19 ± 0.37 | 1.31 ± 0.35 | 0.335 |
| Creatinine, μmol/L | 78.8 ± 23.9 | 69.2 ± 16.1 | 0.190 |

Values are mean ± SD or %. The unpaired Student's *t*-test or chi-square test was performed.

ACEI = angiotensin converting enzyme inhibitor; ARBs = angiotensin II receptor blockers; BMI = body mass index; EF = ejection fraction; HDL = high-density lipoprotein; LDL = low-density lipoprotein.

RUNX2 in VICs incubated with TGFβ by Western blot (Figure 3A) and decreased the protein levels of myofibrogenic markers, including fibronectin, collagen1a, and α smooth muscle actin (αSMA) in the cell lysates (Figures 3B and 3C). Likewise, the down-regulation of PTP1B by siRNA transfection contributed to a decrease in the expression of myofibrogenic markers in TGFβ-treated VICs (Figures 3D and 3E). In addition, TGFβ reversed the alleviation of RUNX2 expression by MSI-1436 in VICs treated with β-GA (Figure 3F), and the phosphorylation level of Smad2 was decreased in VICs treated with MSI-1436 under β-GA medium (Figure 3G). These results suggested that PTP1B might regulate Smad2 phosphorylation to participate in both the TGFβ- and β-GA-induced osteogenic differentiation of VICs.

**MSI-1436 AMELIORATES AORTIC VALVE STENOSIS AND CALCIFICATION IN LDLR$^{-/-}$ mice.** To test the therapeutic potential of PTP1B inhibition in an animal model of CAVD, we fed LDLR$^{-/-}$ mice a normal chow diet and a high-fat diet with saline containing MSI-1436 lactate (10 mg/kg, intraperitoneal, monthly) or DMSO for 24 weeks (Figure 4A). After 24 weeks, the continuous-wave Doppler assessment of aortic valve function indicated that mice in the HFD group showed a significant increase in transvalvular peak jet velocity and mean gradient, whereas MSI-1436 treatment normalized these changes (Figures 4B to 4D). These data indicated that MSI-1436 was effective in protecting against aortic valve stenosis in vivo. The metabolic indexes, such as body weight, high-fat diet intake, blood total triglycerides and cholesterol levels of LDLR$^{-/-}$ mice fed a high-fat diet were shown in Supplemental Figure 3. We then evaluated the morphology of the valve leaflets from different groups and the degree of fibrosis and calcification in aortic valves. H&E staining and Masson's trichrome staining showed that aortic valve leaflet thickness and fibrotic area were increased in the HFD group compared with the normal chow group, which coincided with the calcium nodule formation demonstrated by Von Kossa staining (Figures 4E to 4G). MSI-1436 treatment significantly reduced HFD-induced thickening, fibrosis and calcium deposits in aortic valves (Figures 4E to 4G), indicating the beneficial effects of PTP1B inhibition against aortic valve fibrocalcification in LDLR$^{-/-}$ mice. Consistent with the decreased calcium deposition, mice in the MSI-1436 injection group showed much lower expression of osteogenic markers, including RUNX2 and BMP2, in the aortic valve leaflets than that of HFD mice, as demonstrated by immunofluorescence staining (Figures 4H and 4I). In addition, we identified infiltrating macrophages in the aortic valve leaflets and found that HFD mice showed markedly increased macrophage infiltration, as indicated by the macrophage marker CD68, whereas a reduced number of macrophages was observed in the MSI-1436-treated mice (Figure 4J). Overall, these results suggested that MSI-1436 ameliorated aortic valve calcification in vivo. To avoid the side-effect of PTP1B inhibition on body weight, we evaluated the effect of PTP1B inhibition in the aortic valve wire injury mice model without dietary intervention. Consistent with the aforementioned results in LDLR$^{-/-}$ mice, MSI-1436 treatment was effective in protecting against the increase in transvalvular peak jet velocity and mean gradient via echocardiography and valve thickening via H&E staining in wire injury-induced aortic valve stenosis mice (Supplemental Figure 4).

**MSI-1436 PROTECTS THE MITOCHONDRIAL BIOGENESIS AND FUNCTION IN VIC OSTEOGENESIS.** ROS-mediated oxidative stress had an important role in the pathophysiology of CAVD, inducing the differentiation of VICs into osteoblasts and myofibroblasts, and it was always accompanied by decreased mitochondrial biogenesis and mitochondrial dysfunction. We first assessed the effect of PTP1B inhibition on oxidative stress in VICs cultured in the presence of β-GA and TGFβ. As shown in Figures 5A and 5C, both β-GA and TGFβ treatment stimulated ROS production in VICs, as demonstrated by DCFH-DA staining and flow

**FIGURE 2** Inhibition and Knockdown of PTP1B Prevented β-GA-induced Osteogenic Differentiation of VICs In Vitro

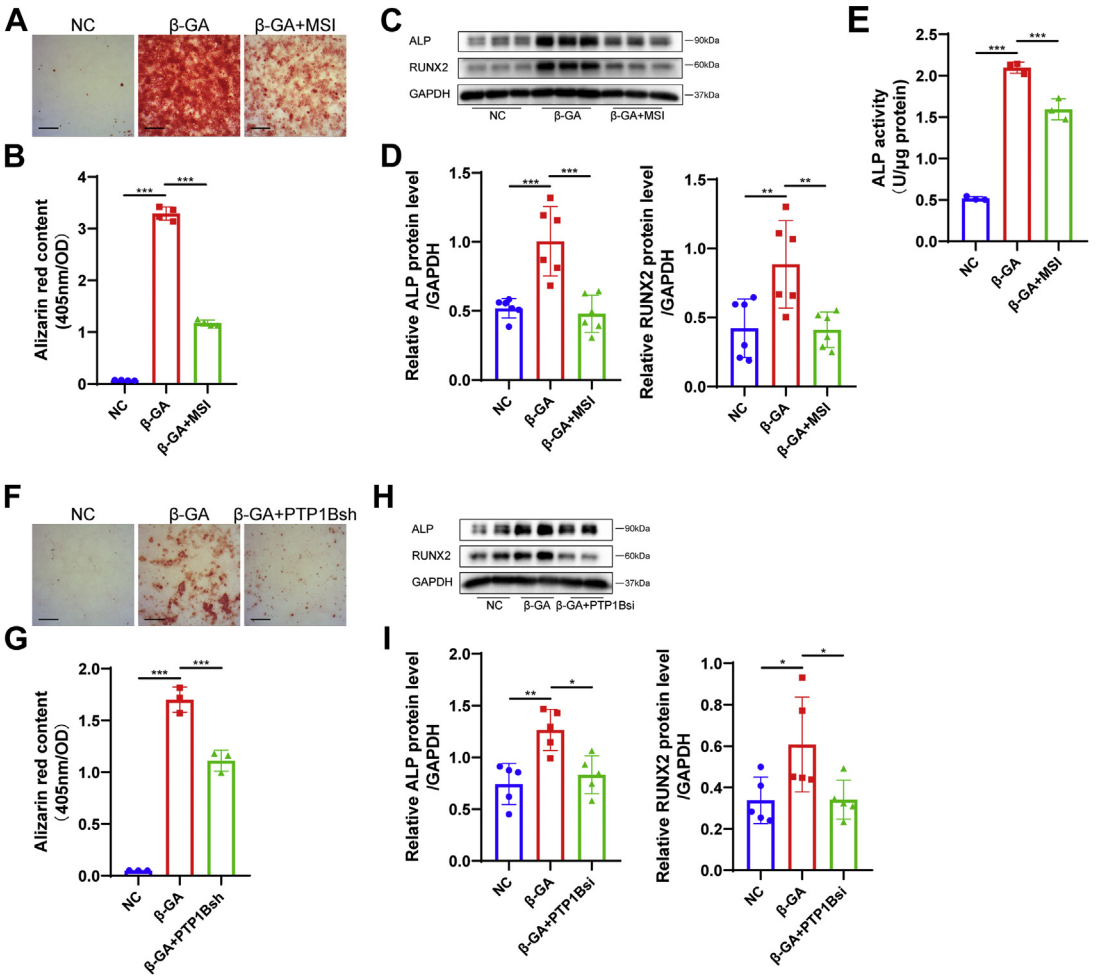


**(A and B)** Calcium nodule formation in human VICs was determined by alizarin red staining **(A)**, and quantitative analysis by 405 nm spectrophotometry **(B)** showed that the PTP1B-specific inhibitor MSI-1436 (MSI, 20 μmol/L) treatment significantly attenuated β-GA-induced calcium nodule formation in VICs in contrast to dimethyl sulfoxide (DMSO) treatment (n = 4). **Scale bar:** 50 μm. **(C and D)** Expression of osteogenic markers, including alkaline phosphatase (ALP) and RUNX2, was assessed by western blot in VICs incubated with β-GA under MSI-1436 or DMSO treatment (n = 6). **(E)** ALP activity was measured using the ALP activity assay kit and normalized to total protein content (n = 3). **(F and G)** Alizarin red staining images **(F)** and quantification results **(G)** of VICs after β-GA treatment in the presence of PTP1B shRNA (PTP1Bsh) or control vector lentivirus transfection (n = 3). **Scale bar:** 50 μm. **(H and I)** Relative ALP and RUNX2 protein levels were decreased in VICs transfected with PTP1B siRNA (PTP1Bsi) in contrast to control vector under β-GA medium (n = 5). Values are mean ± SD. The analysis of variance with Tukey's post hoc test was performed. *$P < 0.05$; **$P < 0.01$; ***$P < 0.001$. Abbreviations as in Figure 2.

cytometry analysis, and MSI-1436 treatment eliminated the increased ROS generation. We subsequently aimed to determine whether these changes influenced mitochondrial biogenesis. To assess mitochondrial morphology, mitochondria were labelled by MitoTracker Deep Red (MitoTracker) staining, and live cell mitochondrial immunofluorescence images indicated that β-GA and TGFβ decreased the fluorescence intensity of mitochondria, whereas MSI-1436 could prevent the decrease in mitochondrial biogenesis (Figures 5B and 5D). We verified these observations through flow cytometry, and the quantitative results showed that treatment with MSI-1436 recovered the mitochondrial decrease in VIC osteogenesis (Figure 5E). The promotion of mitochondrial biogenesis in response to MSI-1436 treatment was further demonstrated by an increase in mitochondrial DNA (mtDNA) mean copy number (Figure 5F). To

**FIGURE 3 MSI-1436 Inhibited TGFβ-Induced Osteogenic and Myofibrogenic Differentiation of VICs In Vitro**

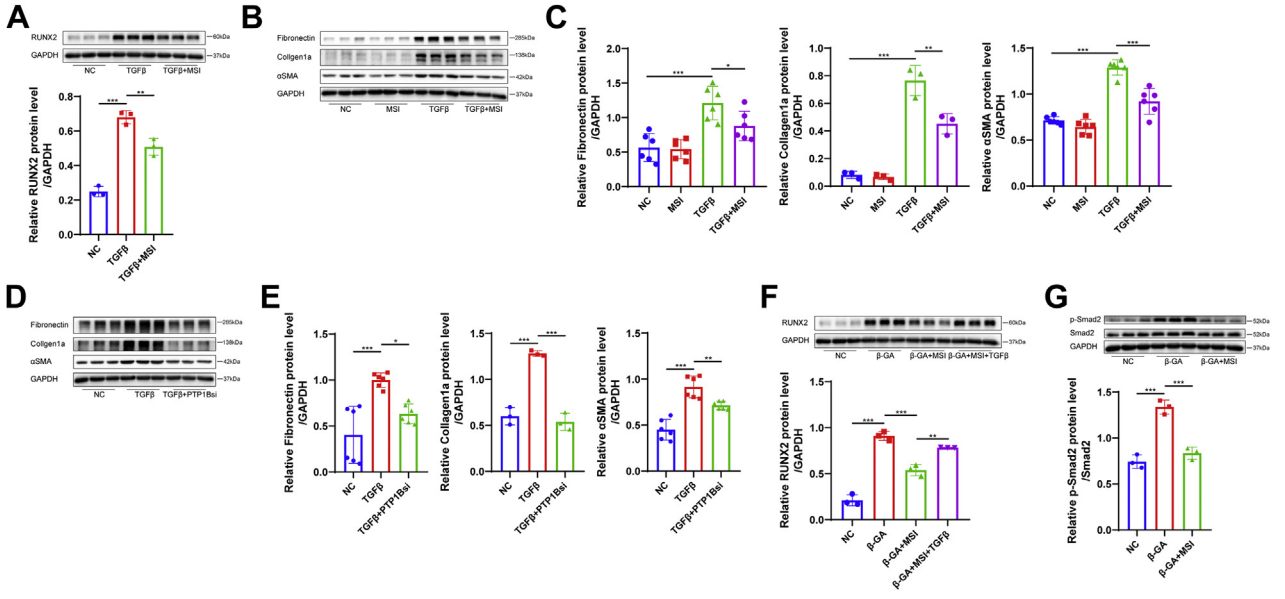


**(A)** The protein level of the osteogenic marker RUNX2 was assessed in TGFβ (10 ng/mL)–treated VICs with MSI-1436 (MSI, 20 μmol/L; n = 3) or DMSO. **(B and C)** Protein levels of the myofibrogenic markers, including fibronectin, collagen1a and αSMA, were assessed in TGFβ-treated VICs with MSI-1436 treatment or DMSO treatment by Western blot (n = 3 or 6). **(D and E)** Relative protein levels of fibronectin, collagen1a, and αSMA were decreased in VICs transfected with PTP1Bsi or control vector under TGFβ medium (n = 3 or 6). **(F)** The addition of TGFβ to VICs treated with MSI-1436 increased RUNX2 expression under β-GA medium (n = 3). **(G)** The relative protein level of p-Smad2 quantified by normalizing to the Smad2 level was decreased in VICs treated with MSI-1436 under β-GA medium (n = 3). Values are mean ± SD. Analysis of variance with Tukey's post hoc test was performed. *$P < 0.05$; **$P < 0.01$; ***$P < 0.001$. Abbreviations as in Figures 1 and 2.

determine the effect of MSI-1436 on mitochondrial function in the VIC osteogenesis, flow cytometry quantitative analysis of tetramethylrhodamine methyl ester (TMRM) and JC-1 staining, which measured the mitochondrial membrane potential, were used and showed that the MSI-1436 group preserved the mitochondrial activity in VICs under osteogenesis (Figures 5G and 5H). In addition, ATP levels in VICs were decreased after β-GA treatment, whereas supplementation with MSI-1436 recovered ATP levels (Figure 5I). These findings indicated that, in addition to promoting the mitochondrial biogenesis, MSI-1436 treatment also resulted in enhanced mitochondrial function in the VICs osteogenesis.

**PTP1B INHIBITION IMPROVES MITOCHONDRIAL DYNAMICS IN VIVO AND REGULATES OPA1 HOMEOSTASIS UNDER OSTEOGENESIS.** To evaluate the effect of PTP1B inhibition on mitochondrial biogenesis in the aortic valve leaflets of LDLR$^{-/-}$ mice, we labelled mitochondria with TOMM20, which is located in the mitochondrial outer membrane. The immunofluorescence results demonstrated that the HFD group had decreased mitochondria in aortic valve compared with that of the normal chow mice, whereas treatment with MSI-1436 preserved mitochondrial number in the presence of HFD (Figures 6A and 6B). Similarly, human calcified valves stained by TOMM20 showed a significant decrease in mitochondrial number compared with that of the normal valves (Figures 6C and 6D). These data suggested that loss of mitochondria after aortic valve calcification and PTP1B inhibition improved mitochondrial dynamics in vivo. Subsequently, to investigate the underlying mechanism by which PTP1B inhibition improved mitochondrial biogenesis in the VICs osteogenesis, we observed the mitochondrial ultrastructure using a transmission electron microscope. VICs cultured under MSI-1436 treatment demonstrated dense and elongated tubular mitochondria with swollen cristae dispersed within the cells, whereas sparse, fewer, and empty mitochondria were observed in β-GA-treated VICs (Figure 6E). We quantified the levels of mRNAs involved in mitochondrial oxidative phosphorylation, including SDHB, ATP5A, NDUFB1, MTCO1, and UQCR10, and quantitative real-time polymerase chain reaction analysis demonstrated there were no significant changes in the components of the mitochondrial electronic respiratory chain among the 3 groups

**FIGURE 4 MSI-1436 Attenuated Aortic Valve Calcification in LDLR$^{-/-}$ Mice**

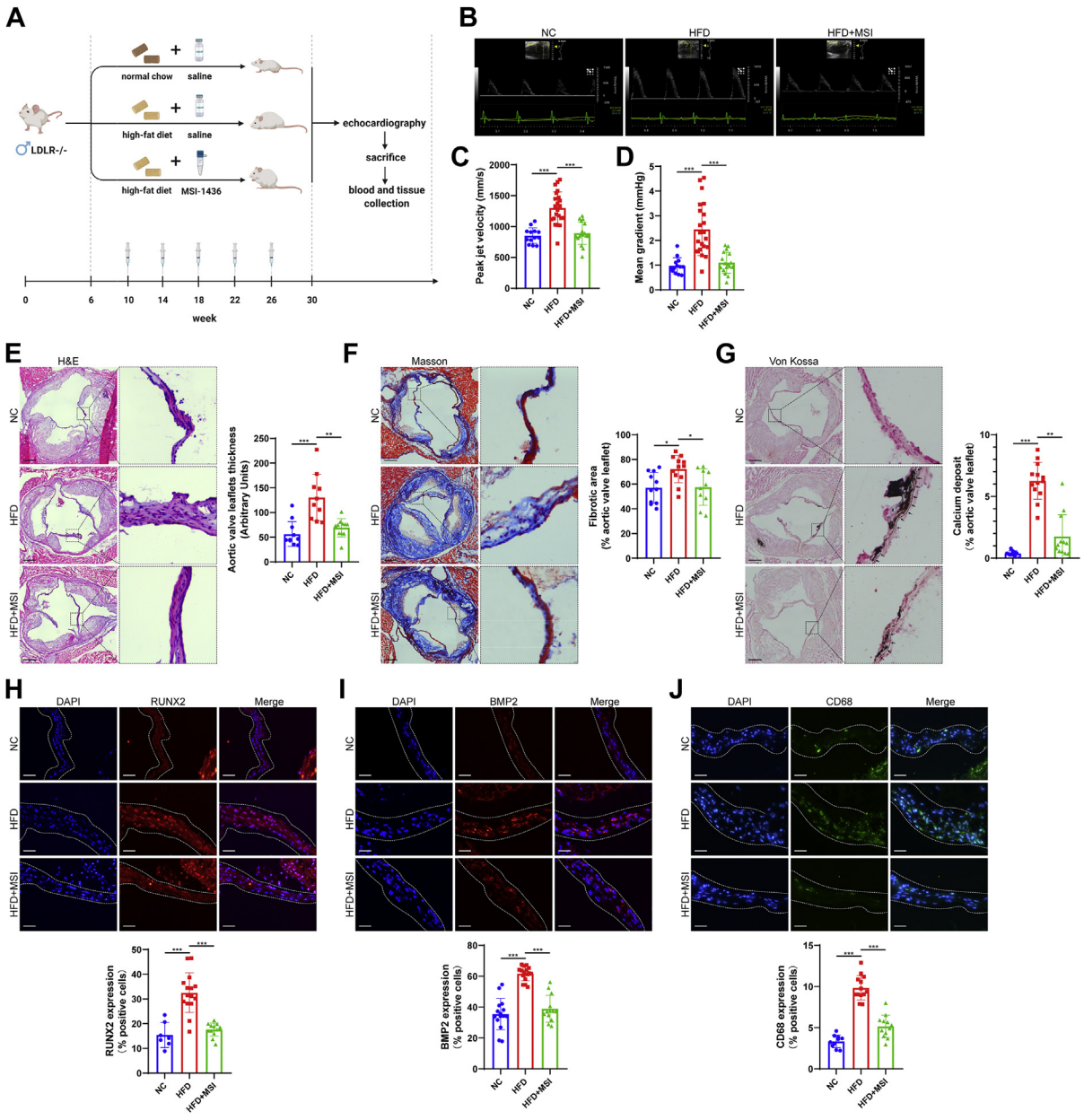


**(A)** Schematic representation of the animal experiments. LDLR$^{-/-}$ male mice were divided into the following: 1) NC, saline with DMSO; 2) HFD, saline with DMSO; and 3) HFD saline with MSI-1436 (10 mg/kg, intraperitoneally, monthly). **(B)** Representative echocardiographic images of LDLR$^{-/-}$ mice fed a NC and an HFD with saline containing MSI-1436 or DMSO injection after 24 weeks. **(C and D)** Continuous-wave Doppler assessment of the aortic valve function indicated that mice in the HFD group (n = 22) showed a significant increase in transvalvular peak jet velocity **(C)** and mean gradient **(D)** compared with that of the NC group (n = 13), whereas MSI-1436 treatment (n = 17) reversed these changes. **(E to G)** Representative H&E staining, Masson's trichrome staining (Masson), and Von Kossa staining images of aortic valves in LDLR$^{-/-}$ mice from different groups. **Scale bar:** 150 μm. Quantitative analysis of valve leaflet thickness **(E)** (n = 11, 10, 11), fibrosis **(F)** (n = 11, 12, 10), and calcium nodule deposits **(G)** (n = 10, 13, 12) was assessed by ImageJ. **(H to J)** Representative immunofluorescence staining images of osteogenic markers, including RUNX2 and BMP2, and the macrophage marker CD68 in aortic valve sections. **Scale bar:** 15 μm. MSI-1436 injection showed much fewer RUNX2 **(H)** (n = 7, 15, 13), BMP2 **(I)** (n = 15, 16, 13), and CD68 **(J)** (n = 10, 13, 12)-positive cells in aortic valves than HFD-fed mice. Values are mean ± SD. The Kruskal-Wallis test was performed for **E and G**, and analysis of variance with Tukey's post hoc test was performed for **C, D, F, H, I, and J**. *$P < 0.05$; **$P < 0.01$; ***$P < 0.001$. Abbreviations as in Figures 1 and 2.

**FIGURE 5 MSI-1436 Preserved Mitochondrial Homeostasis in the Osteogenic Differentiation of VICs**

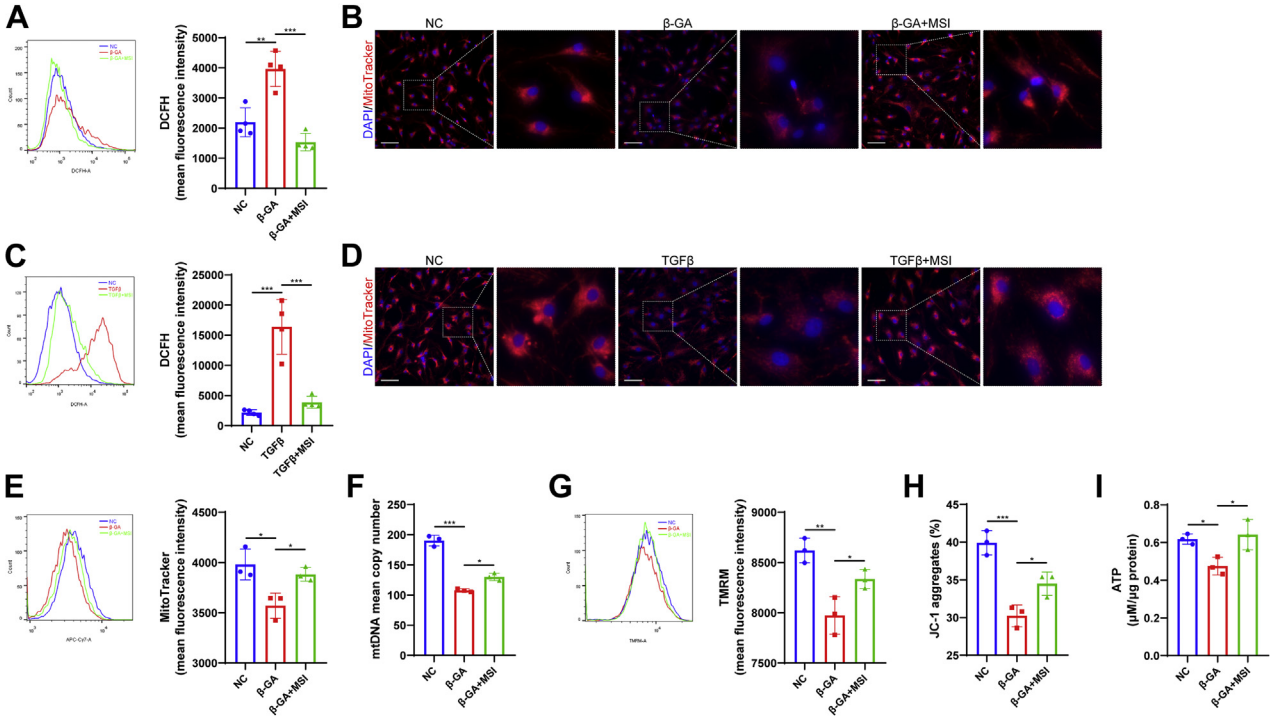


**(A)** The level of cellular reactive oxygen species (ROS) was detected by flow cytometry with DCFH-DA staining, and quantification of the mean fluorescence intensity of DCFH showed that MSI-1436 treatment decreased ROS generation in VICs cultured in β-GA medium (n = 4). **(B)** Representative MitoTracker Deep Red (MitoTracker) staining images of VICs treated with β-GA medium in the presence of MSI-1436 were used to observe mitochondrial morphology. **Scale bar:** 20 μm. **(C and D)** The level of ROS **(C)** and representative MitoTracker staining images **(D)** of VICs under TGFβ medium with or without MSI-1436 treatment. **(E)** Quantitative analysis of MitoTracker staining by flow cytometry showed that MSI-1436 reversed the mitochondrial mass decrease in VICs caused by β-GA treatment (n = 3). **(F)** Quantitative real-time polymerase chain reaction was performed to quantify the mitochondrial DNA (mtDNA) mean copy number, which was normalized to nuclear DNA level (n = 3). **(G and H)** Quantification of the mean fluorescence intensity of tetramethylrhodamine methyl ester (TMRM) staining **(G)** and the percentage of JC-1 aggregates **(H)** by flow cytometry showed that MSI-1436 treatment increased the mitochondrial membrane potential in VIC osteogenesis (n = 3). **(I)** Cellular ATP levels in VICs treated with or without MSI-1436 under β-GA medium were measured through a luciferase-based assay, and the data were calibrated with total protein content (n = 3). Values are mean ± SD. The analysis of variance with Tukey's post hoc test was performed. *$P < 0.05$; **$P < 0.01$; ***$P < 0.001$. Abbreviations as in Figures 1 and 2.

(Figure 6F). To further investigate the changes in mitochondrial dynamics regulated by PTP1B inhibition in VICs, we measured the levels of the following pivotal proteins involved in mitochondrial dynamics: dynamin-related protein 1 (DRP1), which is responsible for mitochondrial fission, and optic atrophy 1 (OPA1), which is responsible for fusion. Although no significant difference was detected for DRP1 after MSI-1436 treatment (Figure 6G), the augment on long form of OPA1 (L-OPA1) expression was observed in the β-GA group, whereas the short form of OPA1 (S-OPA1) was increased after MSI-1436 treatment during osteogenesis (Figure 6H). These results indicated that the ratio of L-OPA1 to S-OPA1, which contributed to mitochondrial dynamics, might influence osteogenic differentiation of VICs.

**PTP1B INHIBITION PREVENTS THE VICs OSTEOGENESIS BY DIRECTLY INTERACTING WITH THE OPA1 ISOFORM TRANSITION.** Although human OPA1 had 8 different mRNA splice variants according to various combinations of exon 4b, exon 5, and exon 5b, the short isoforms were produced by proteolytic cleavage of the long isoform by OMA1 (cleaved at the $S_1$ site encoded by exon 5) and YME1L1 (cleaved at the $S_2$ site encoded by the alternative exon 5b). Variants that contained exon 4b ($S_3$ site) were such avid substrates for proteolytic processing that they generated only short isoforms. To determine the effect of L- and S-OPA1 on VIC osteogenesis, we used lentivirus expressing the OPA1v1, which contains only the $S_1$ site, to overexpress L-OPA1 in VICs (Figures 7A and 7B). OPA1v8 contained exon 4b, which allowed complete cleavage

**FIGURE 6 PTP1B Inhibition Preserved Mitochondrial Dynamics In Vivo and Regulated OPA1 Isoform Transition in VIC Osteogenesis**

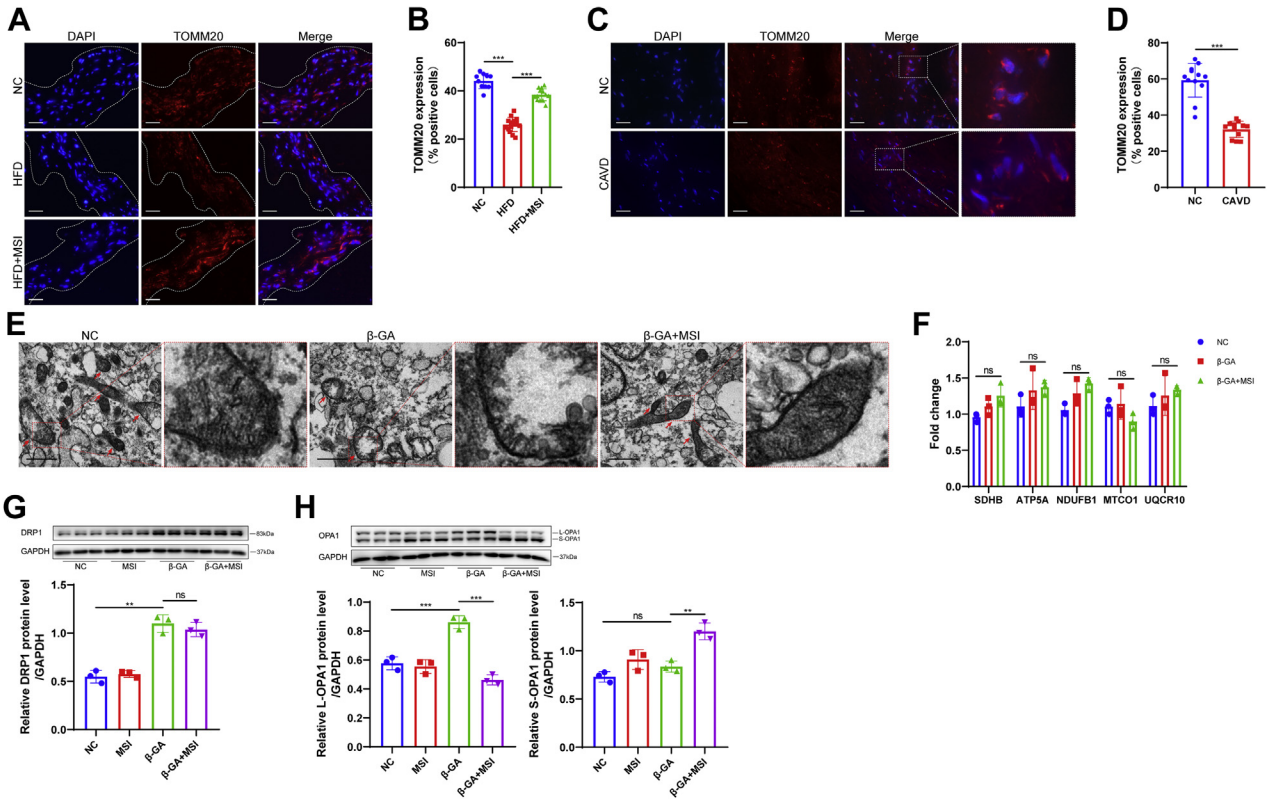


**(A)** Representative immunofluorescence images of mitochondria stained by the mitochondrial marker TOMM20 in aortic valve leaflets of $LDLR^{-/-}$ mice in different groups. **Scale bar:** 15 μm. **(B)** Quantification of the percentage of TOMM20-positive cells showed that MSI-1436 treatment (n = 13) reversed the depletion in mitochondrial number in the presence of HFD (n = 15). **(C)** Representative mitochondrial immunofluorescence staining images of human normal valves and calcified aortic valves. **Scale bar:** 15 μm. **(D)** Quantitative analysis showed fewer mitochondria in CAVD vs the normal control subjects (n = 12). **(E)** Mitochondrial morphology was observed by a transmission electron microscope, and representative images showed significant changes in the mitochondrial number and morphology in VIC osteogenesis after MSI-1436 treatment. **Scale bar:** 1 μm. **(F)** Quantification of electronic respiratory chain-related genes by quantitative real-time polymerase chain reaction was normalized to ACTIN level (n = 3). **(G and H)** Protein levels of mitochondrial dynamics-related proteins, including DRP1 **(G)** and long form of OPA1 (L-OPA1) and short form of OPA1 (S-OPA1) **(H)**, were determined by Western blot (n = 3). Values are mean ± SD. The unpaired Student's *t*-test was performed for **D** and analysis of variance with Tukey's post hoc test was performed for **B, F, G, and H**. $^{**}P < 0.01$; $^{***}P < 0.001$; ns = not significant. Abbreviations as in **Figures 1 and 2**.

of L-OPA1 into S-OPA1, while VICs transfected with OPA1v7 lentivirus, which contained $S_1$ and $S_2$ cleavage sites, overexpressed both L- and S-OPA1 (**Figures 7A and 7B**). In the presence of OPA1v1 or control vector in VICs, L-OPA1 overexpression had the ability to promote RUNX2 expression under osteogenic medium treatment (**Figure 7C**). However, we found a significant decrease in RUNX2 expression in VICs transfected with OPA1v8 and OPA1v7 lentiviruses, which overexpressed exclusive S-OPA1 and both long and short forms (**Figures 7D and 7E**). By comparing OPA1v1 with OPA1v7 in terms of OPA1 expression, we discovered that L-OPA1 was mostly cleaved at the $S_2$ site by YME1L1 in VICs. Hence, to further explore the role of the ratio of long and short isoforms in VIC osteogenesis, the knockdown of YME1L1 by siRNA was examined and found to up-regulate the expression of L-OPA1 (Supplemental Figure 2C) and aggravate the osteogenesis of VICs under β-GA treatment (**Figure 7F**). However, YME1L1 overexpression in VICs alleviated osteogenesis induced by β-GA (**Figure 7G**). Knockdown of OMA1 by siRNA increased RUNX2 protein expression in VICs under β-GA treatment (Supplemental Figure 5D). There were no significant differences in either the mRNA or protein levels of YME1L1 and OMA1 in β-GA-treated VICs after MSI-1436 treatment (Supplemental Figures 5A and 5B). To further investigate the mechanism of how PTP1B acted on OPA1 cleavage, we then performed an immunoprecipitation assay to test the interaction

**FIGURE 7 PTP1B Inhibition Prevented VIC Osteogenesis by Directly Interacting With the Transition of the OPA1 Isoform**

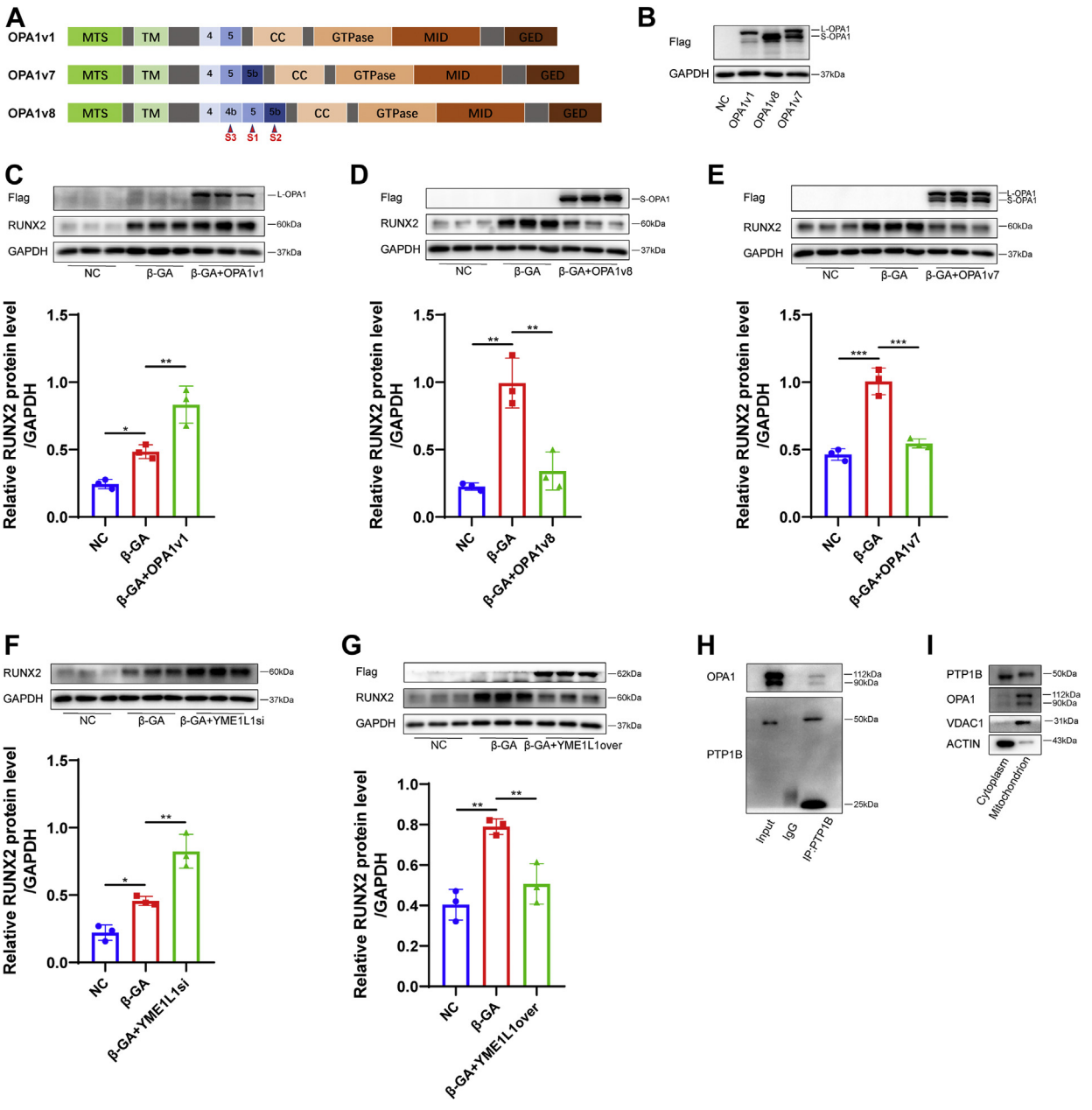


**(A)** OPA1 proteolytic cleavages occurred at $S_1$, $S_2$, and $S_3$ in exons 5, 5b, and 4b. Variant 1 (OPA1v1) contained the $S_1$ site, whereas OPA1 variant 7 (OPA1v7) contained an extra $S_2$ site. Variant 8 (OPA1v8) contained all 3 cleavage sites. **(B)** Three OPA1 variants were overexpressed in VICs, and Western blot of cell lysates from these cells showed exclusive overexpression of L- and S-OPA1 in VICs expressing OPA1v1 and OPA1v8 in contrast to control vector lentivirus, respectively, and the presence of both L- and S-OPA1 in cells expressing OPA1v7. **(C to E)** The relative protein level of RUNX2 in VICs transfected with OPA1v1 **(C)**, OPA1v8 **(D)**, and OPA1v7 **(E)** under β-GA treatment was assessed by Western blot (n = 3). **(F)** The relative RUNX2 protein level was increased in VICs transfected with YME1L1 siRNA (YME1L1si) or control vector under β-GA medium (n = 3). **(G)** The protein level of RUNX2 was decreased in VICs overexpressing YME1L1 (YME1L1over) under β-GA medium (n = 3). **(H)** Immunoprecipitation analysis of VICs with monoclonal anti-PTP1B antibody showed exclusive OPA1 protein expression in the immunoprecipitation group vs the IgG group. **(I)** Western blot analysis of PTP1B in the cytoplasm and mitochondria. The lysate of mitochondria was normalized to VDAC1 level, and the lysate of cytoplasm was normalized to ACTIN level. Values are mean ± SD. The analysis of variance with Tukey's post hoc test was performed. *$P < 0.05$; **$P < 0.01$; ***$P < 0.001$. CC = coiled-coil domain; GED = GTPase effector domain; MID = middle domain; MTS = N-terminal mitochondrial targeting sequence; TM = transmembrane; other abbreviations as in Figures 1 and 2.

between endogenous PTP1B and OPA1. As expected, PTP1B interacted with OPA1 directly in VICs (**Figure 7H**). Because it was widely believed that PTP1B anchored at the endoplasmic reticulum membrane, we next intended to determine if there was PTP1B that anchored at the mitochondrial membrane in human VICs. A certain amount of PTP1B existed in mitochondria (**Figure 7I**), which additionally indicated that PTP1B might have a direct interaction with OPA1.

## DISCUSSION

Calcific aortic valve disease is a progressive disease in which the end stage is characterized by thickening, fibrosis, and calcification in the aortic valve leaflets, resulting in left ventricular outflow obstruction and heart failure. Clinical factors, such as age, sex, obesity, smoking, diabetes, and dyslipidemia, participated in the initiation and progression of aortic valve calcification.[1] In the present work, because most of the normal valve samples were obtained from patients with dilated cardiomyopathy and cerebral hemorrhage whose aortic valves were thin and had lack of calcification, there were differences in age and left ventricular ejection fraction between the noncalcified and calcified groups. Besides, there were no significant differences in body mass index, total triglycerides, total cholesterol, low-density lipoprotein, or high-density lipoprotein between the NC and CAVD patients. VICs were the most prevalent cell type in aortic valves and were essential for valvular homeostasis and remodeling during the pathological process of CAVD.[31] It was worth noting that we also documented that PTP1B was increased in VICs isolated from calcified valves vs normal valves. In addition to media containing organic phosphate (β-GA), media containing high inorganic phosphate ($Na_2HPO_4$) also induced the osteogenesis of VICs in vitro.[32] We found that PTP1B was increased in VICs under organic phosphate treatment rather than inorganic phosphate treatment. Therefore, we developed aortic valve calcification in vivo through $LDLR^{-/-}$ mice instead of a chronic kidney disease mouse model, and we found an increased expression of PTP1B in the aortic valve leaflets from the HFD group.

CAVD is often termed a fibrocalcific disease because a hallmark of CAVD initiation is collagen accumulation that leads to sclerotic leaflet. Ectopic calcium deposits forming within these stiffened valves further decreased tissue compliance, eventually resulting in valve stenosis.[33] The initiation of the myofibrogenic and osteogenic differentiation of VICs seemed to be regulated by TGFβ, which were involved in the collagen deposition and calcification of valve leaflets.[34] In the current work, PTP1B inhibition with MSI-1436 inhibited VIC differentiation toward myofibroblast and osteoblast phenotypes under the addition of TGFβ. The capability and efficacy of MSI-1436 in alleviating both valvular fibrosis and calcium nodule formation in vitro made this PTP1B inhibitor particularly interesting and encouraging to assess as a potential therapy for this debilitating disease in vivo.

The key to treating PTP1B-associated diseases is to develop potent and selective PTP1B inhibitors. However, because of the high similarity of different protein tyrosine phosphatases, it was still a daunting challenge, and developing both safe and effective PTP1B inhibitors that could be used in clinical trials was emerging as a popular topic.[13] MSI-1436 was a specific, reversible, and noncompetitive inhibitor of PTP1B that preferentially targeted the long form of PTP1B (1-405), containing the extended C-terminal segment,[35] and it has completed phase I of clinical trials for diabetes treatment (NCT00806338). PTP1B was reported to be widely and highly expressed in cardiovascular system cells, such as endothelial cells, vascular smooth muscle cells and cardiomyocytes.[36] A recent study found that the use of MSI-1436 every 3 days at 1.25 mg/kg could stimulate regeneration of cardiomyocytes in adult mouse hearts following ischemic injury without inducing significant changes in body weight,[15] which indicated the effectiveness and specificity of MSI-1436 usage in heart. Above all, to reduce the side-effect of MSI-1436 on body weight and maintain its specific effect on the cardiovascular system, we prolonged the injection interval (monthly) of MSI-1436 compared with that of a previous description (weekly).[35] In the present study, the administration of MSI-1436 decreased the expression of RUNX2 and BMP2 in the aortic valve of the $LDLR^{-/-}$ mice fed a high-fat diet. In addition, PTP1B inhibition also alleviated the deposition of calcium and fibrotic areas in aortic valve leaflets and decelerated the development of aortic valve stenosis after HFD. To validate that the beneficial effects of PTP1B inhibition were independent of its potential influence on body weight, a second model of aortic valve stenosis was therefore established for this study by using C57BL/6 mice and applying the protocol of aortic valve wire injury introduced by Honda et al[37] and called severe injury by Niepmann et al.[38] Indeed, these experiments demonstrated decreased peak jet velocity and aortic valve leaflet thickness after MSI-1436 treatment in wire injury mice, hence confirming that the beneficial effects on aortic valve disease mediated through PTP1B inhibition were

reproducible also under normolipidemic conditions and in the absence of dietary intervention.

It was well-established that oxidative stress was a critical pathophysiological component of numerous cardiovascular diseases, including inflammation, metabolic disorder, and atherosclerosis,[39] which were all risk factors for CAVD.[40] Several ROS sources might, in principle, contribute to ROS production and scavenging, including mitochondria, superoxide dismutase, and NOX enzymes. Among these sources, substantial studies have indicated that mitochondrial dysfunction played a central role in cardiovascular calcification pathophysiology.[41] Failure of the normal processes controlled by mitochondria led to abnormal ROS production, calcium homeostasis, the peroxidation of proteins and lipids, and the activation of mitochondrial-driven cell death, which were considered biological processes that led to the initiation and progression of cardiovascular calcification.[42-44] A recent study found a new role for DRP1, a key protein that controls mitochondrial fission, in calcified human aortic valves, where its RNA-mediated interference in VICs was able to reduce the calcification process through an increase in SRY-box transcription factor 9 expression.[45] From these studies, a broader understanding of the mechanisms of mitochondria in VIC osteogenesis might further the development of new therapeutic strategies for CAVD. In addition, it was reported PTP1B regulated Src activity on oxidative phosphorylation in rat brain mitochondria,[46] which indicated that PTP1B might play an important role in modulating mitochondrial function. However, the association between PTP1B and mitochondrial homeostasis in valvular calcification remains unknown. In this study, MSI-1436 treatment eliminated the generation of ROS in VICs incubated with β-GA and TGFβ. The increase in mitochondrial biogenesis in response to MSI-1436 treatment was further confirmed by MitoTracker staining and mtDNA mean copy number. Flow cytometry analysis of TMRM and JC-1 staining showed that the MSI-1436 group improved mitochondrial function in the VIC osteogenesis. In addition, depletion of mitochondria was found in aortic valve calcification, and PTP1B inhibition preserved mitochondrial dynamics in vivo. Collectively, these novel findings provided a mitochondrial pathway by which PTP1B inhibition alleviated aortic valve calcification in vitro and in vivo.

OPA1 is a dynamin-related protein associated with the inner mitochondrial membrane and functions in mitochondrial inner membrane fusion and crista maintenance.[47] There were currently 2 general models explaining how long and short OPA1 isoforms regulate mitochondrial fusion activity. The first model indicated that under specific cellular conditions, L-OPA1 alone could have substantial fusion activity, whereas S-OPA1 has instead been suggested to have fission activity based on the observation that overexpression of S-OPA1 led to mitochondrial fragmentation.[48] The other study observed that the expression of L- or S-OPA1 alone resulted in very low mitochondrial fusion activity and that the fusion robust levels required a combination of both the long and short forms.[49,50] In addition, S-OPA1 contained all of the dynamin protein functional domains, suggesting that S-OPA1 had a physiological role, including maintaining cristae and energetics through its GTPase activity.[51] Furthermore, a recent study showed that the absence of S-OPA1 markedly increased oxidant-induced cell death under oxidative phosphorylation conditions, which indicated that S-OPA1 generation was necessary for supporting cell survival.[52] In our study, we found that exclusive L-OPA1 overexpression promoted RUNX2 expression in VICs osteogenesis. In contrast, there was a significant decrease in RUNX2 expression in the VICs overexpressing exclusive S-OPA1 and both long and short forms. Therefore, the ratio of L- and S-OPA1 influenced the VICs osteogenesis. As YME1L1 and OMA1 levels were not altered in β-GA-treated VICs after MSI-1436 treatment, the role of PTP1B inhibition on OPA1 isoform transition was independent of the interaction on YME1L1 or OMA1. In addition, we found that PTP1B interacted with OPA1 directly by using an IP assay. It was reported that PTP1B was located in rat brain mitochondria and modulated the Src regulation of oxidative phosphorylation in mitochondria.[46] In the present work, we found PTP1B existence in isolated VIC mitochondria, which further demonstrated the possibility of interaction between PTP1B and OPA1.

**STUDY LIMITATIONS.** There are various disease stages in patients with aortic valve stenosis, including risky, progressive, asymptomatic, symptomatic with a high gradient, and symptomatic with a low gradient. The CAVD samples were all from patients with severe stenosis who needed to be treated with valve replacement. Hence, we could not rule out that PTP1B elevation might occur later during the progression from an asymptomatic initial phase of the disease to severe stenosis. In addition, we do not provide evidence suggesting the role of conditional PTP1B knockout mice in aortic valve calcification, which can avoid the side effects of global PTP1B inhibition, because there is no valvular cell-specific knockout marker currently, and this would need to be crossbred with $LDLR^{-/-}$ or $ApoE^{-/-}$ mice that develop CAVD. Nonetheless, the present findings in

human calcified aortic valves and primary human aortic VICs indicate that PTP1B inhibitor is a novel pharmacotherapy that contributes to ameliorate CAVD.

## CONCLUSIONS

In this work, we found that the up-regulation of PTP1B was critically involved in aortic valve calcification. MSI-1436 was effective in alleviating the osteogenic and myofibrogenic differentiation of VICs in vitro and mitigated aortic valve fibrocalcification and stenosis in a diet-induced mouse model of CAVD. In addition, we reported the function of PTP1B in regulating mitochondrial homeostasis in CAVD and further showed that mitochondrial dynamics mediated by OPA1 contributed to the osteogenesis process in VICs. Therefore, our findings have determined that PTP1B inhibitors offer potential alterative, pharmacological-based therapies for the treatment of CAVD.

## FUNDING SUPPORT AND AUTHOR DISCLOSURES

This work was supported by the National Natural Science Foundation of China (81770252 to Dr Liu, 82030014 and 81870292 to Dr Wang), National Key R&D Program of China (2019YFA0110400 and 2016YFC1301204 to Dr Wang), and the Key R&D Program of Zhejiang Province Science and Technology Department (2021C03097 and 2018C03084 to Dr Wang). Dr Xinyang Hu, a member of the Department of Cardiology from our hospital, provided some funds she received for routine maintenance of our lab (2017YFA0103700).

The authors have reported that they have no relationships relevant to the contents of this paper to disclose.

**ADDRESS FOR CORRESPONDENCE:** Dr Xianbao Liu, Department of Cardiology, The Second Affiliated Hospital, School of Medicine, Zhejiang University, 88 Jiefang Road, Hangzhou 310009, China. E-mail: liuxb@zju.edu.cn.

## PERSPECTIVES

**COMPETENCY IN MEDICAL KNOWLEDGE:** Due to the absence of effective pharmacotherapies alleviating CAVD progression, PTP1B inhibition protects against the fibrocalcific response in VICs and both fibrosis, an earlier pathological process in CAVD progression, and calcification in CAVD, which provides a theoretical advantage to prevent CAVD development compared with targeting other pathways that affect calcification alone.

**TRANSLATIONAL OUTLOOK:** We identified PTP1B as a key regulator of the etiology of CAVD and VIC osteogenesis. In addition to the need to overcome the challenges inherent to synthesizing potent and selective small molecule inhibitors for PTP1B, it is crucial to also develop novel approaches to specifically target tissues of interest, such as the cardiovascular system, to optimize the clinical benefits of inhibiting PTP1B while reducing the risk of potential off-target side effects.

## REFERENCES

**1.** Otto CM, Prendergast B. Aortic-valve stenosis—from patients at risk to severe valve obstruction. *N Engl J Med*. 2014;371:744–756.

**2.** Leon MB, Smith CR, Mack M, et al. Transcatheter aortic-valve implantation for aortic stenosis in patients who cannot undergo surgery. *N Engl J Med*. 2010;363:1597–1607.

**3.** Makkar RR, Thourani VH, Mack MJ, et al. Five-year outcomes of transcatheter or surgical aortic-valve replacement. *N Engl J Med*. 2020;382:799–809.

**4.** Rajamannan NM, Evans FJ, Aikawa E, et al. Calcific aortic valve disease: not simply a degenerative process: a review and agenda for research from the National Heart and Lung and Blood Institute Aortic Stenosis Working Group. Executive summary: calcific aortic valve disease-2011 update. *Circulation*. 2011;124:1783–1791.

**5.** Yan AT, Koh M, Chan KK, et al. Association between cardiovascular risk factors and aortic stenosis: the CANHEART Aortic Stenosis Study. *J Am Coll Cardiol*. 2017;69:1523–1532.

**6.** Rossebo AB, Pedersen TR, Boman K, et al. Intensive lipid lowering with simvastatin and ezetimibe in aortic stenosis. *N Engl J Med*. 2008;359:1343–1356.

**7.** Schlotter F, de Freitas RCC, Rogers MA, et al. ApoC-III is a novel inducer of calcification in human aortic valves. *J Biol Chem*. 2021;296:100193. https://doi.org/10.1074/jbc.RA120.015700

**8.** Bouchareb R, Boulanger MC, Tastet L, et al. Activated platelets promote an osteogenic programme and the progression of calcific aortic valve stenosis. *Eur Heart J*. 2019;40:1362–1373.

**9.** Baratchi S, Zaldivia MTK, Wallert M, et al. Transcatheter aortic valve implantation represents an anti-inflammatory therapy via reduction of shear stress-induced, piezo-1-mediated monocyte activation. *Circulation*. 2020;142:1092–1105.

**10.** Rutkovskiy A, Malashicheva A, Sullivan G, et al. Valve interstitial cells: the key to understanding the pathophysiology of heart valve calcification. *J Am Heart Assoc*. 2017;6(9):e006339. https://doi.org/10.1161/JAHA.117.006339

**11.** Bellomo E, Birla Singh K, Massarotti A, Hogstrand C, Maret W. The metal face of protein tyrosine phosphatase 1B. *Coord Chem Rev*. 2016;327-328:70–83.

**12.** Elchebly M, Payette P, Michaliszyn E, et al. Increased insulin sensitivity and obesity resistance in mice lacking the protein tyrosine phosphatase-1B gene. *Science*. 1999;283:1544–1548.

**13.** Sharma B, Xie L, Yang F, et al. Recent advance on PTP1B inhibitors and their biomedical applications. *Eur J Med Chem*. 2020;199:112376.

**14.** Gogiraju R, Schroeter MR, Bochenek ML, et al. Endothelial deletion of protein tyrosine phosphatase-1B protects against pressure overload-induced heart failure in mice. *Cardiovasc Res*. 2016;111:204–216.

**15.** Smith AM, Maguire-Nguyen KK, Rando TA, Zasloff MA, Strange KB, Yin VP. The protein tyrosine phosphatase 1B inhibitor MSI-1436 stimulates regeneration of heart and multiple other tissues. *NPJ Regen Med*. 2017;2:4.

**16.** Coquerel D, Neviere R, Delile E, et al. Gene deletion of protein tyrosine phosphatase 1B protects against sepsis-induced cardiovascular dysfunction and mortality. *Arterioscler Thromb Vasc Biol*. 2014;34:1032–1044.

**17.** Thompson D, Morrice N, Grant L, et al. Pharmacological inhibition of protein tyrosine phosphatase 1B protects against atherosclerotic plaque formation in the LDLR(-/-) mouse model of atherosclerosis. *Clin Sci (Lond)*. 2017;131:2489–2501.

**18.** Thompson D, Morrice N, Grant L, et al. Myeloid protein tyrosine phosphatase 1B (PTP1B) deficiency protects against atherosclerotic plaque

formation in the ApoE(-/-) mouse model of atherosclerosis with alterations in IL10/AMPKalpha pathway. *Mol Metab*. 2017;6:845–853.

**19.** Greenberg HZE, Zhao G, Shah AM, Zhang M. Role of oxidative stress in calcific aortic valve disease and its therapeutic implications. *Cardiovasc Res*. 2022;118(6):1433–1451. https://doi.org/10.1093/cvr/cvab142

**20.** Pawade TA, Newby DE, Dweck MR. Calcification in aortic stenosis: the skeleton key. *J Am Coll Cardiol*. 2015;66:561–577.

**21.** New SE, Aikawa E. Molecular imaging insights into early inflammatory stages of arterial and aortic valve calcification. *Circ Res*. 2011;108:1381–1391.

**22.** Das D, Holmes A, Murphy GA, et al. TGF-beta1-Induced MAPK activation promotes collagen synthesis, nodule formation, redox stress and cellular senescence in porcine aortic valve interstitial cells. *J Heart Valve Dis*. 2013;22:621–630.

**23.** Liberman M, Bassi E, Martinatti MK, et al. Oxidant generation predominates around calcifying foci and enhances progression of aortic valve calcification. *Arterioscler Thromb Vasc Biol*. 2008;28:463–470.

**24.** Miller JD, Chu Y, Brooks RM, Richenbacher WE, Pena-Silva R, Heistad DD. Dysregulation of antioxidant mechanisms contributes to increased oxidative stress in calcific aortic valvular stenosis in humans. *J Am Coll Cardiol*. 2008;52:843–850.

**25.** Ortiz C, Caja L, Bertran E, et al. Protein-tyrosine phosphatase 1B (PTP1B) deficiency confers resistance to transforming growth factor-beta (TGF-beta)-induced suppressor effects in hepatocytes. *J Biol Chem*. 2012;287:15263–15274.

**26.** Bourebaba L, Kornicka-Garbowska K, Al Naem M, Rocken M, Lyczko J, Marycz K. MSI-1436 improves EMS adipose derived progenitor stem cells in the course of adipogenic differentiation through modulation of ER stress, apoptosis, and oxidative stress. *Stem Cell Res Ther*. 2021;12:97.

**27.** Gao C, Hu W, Liu F, et al. Aldo-keto reductase family 1 member B induces aortic valve calcification by activating hippo signaling in valvular interstitial cells. *J Mol Cell Cardiol*. 2021;150:54–64.

**28.** Wang Y, Han D, Zhou T, et al. Melatonin ameliorates aortic valve calcification via the regulation of circular RNA CircRIC3/miR-204-5p/DPP4 signaling in valvular interstitial cells. *J Pineal Res*. 2020;69:e12666.

**29.** Simard L, Côté N, Dagenais F, et al. Sex-related discordance between aortic valve calcification and hemodynamic severity of aortic stenosis: is valvular fibrosis the explanation? *Circ Res*. 2017;120:681–691.

**30.** Choi B, Lee S, Kim SM, et al. Dipeptidyl peptidase-4 induces aortic valve calcification by inhibiting insulin-like growth factor-1 signaling in valvular interstitial cells. *Circulation*. 2017;135:1935–1950.

**31.** Liu AC, Joag VR, Gotlieb AI. The emerging role of valve interstitial cell phenotypes in regulating heart valve pathobiology. *Am J Pathol*. 2007;171:1407–1418.

**32.** Back M, Michel JB. From organic and inorganic phosphates to valvular and vascular calcifications. *Cardiovasc Res*. 2021;117(9):2016–2029.

**33.** Weiss RM, Miller JD, Heistad DD. Fibrocalcific aortic valve disease: opportunity to understand disease mechanisms using mouse models. *Circ Res*. 2013;113:209–222.

**34.** Varshney R, Murphy B, Woolington S, et al. Inactivation of platelet-derived TGF-beta1 attenuates aortic stenosis progression in a robust murine model. *Blood Adv*. 2019;3:777–788.

**35.** Lantz KA, Hart SG, Planey SL, et al. Inhibition of PTP1B by trodusquemine (MSI-1436) causes fat-specific weight loss in diet-induced obese mice. *Obesity (Silver Spring)*. 2010;18:1516–1523.

**36.** Thiebaut PA, Besnier M, Gomez E, Richard V. Role of protein tyrosine phosphatase 1B in cardiovascular diseases. *J Mol Cell Cardiol*. 2016;101:50–57.

**37.** Honda S, Miyamoto T, Watanabe T, et al. A novel mouse model of aortic valve stenosis induced by direct wire injury. *Arterioscler Thromb Vasc Biol*. 2014;34:270–278.

**38.** Niepmann ST, Steffen E, Zietzer A, et al. Graded murine wire-induced aortic valve stenosis model mimics human functional and morphological disease phenotype. *Clin Res Cardiol*. 2019;108:847–856.

**39.** Forrester SJ, Kikuchi DS, Hernandes MS, Xu Q, Griendling KK. Reactive Oxygen Species in Metabolic and Inflammatory Signaling. *Circ Res*. 2018;122:877–902.

**40.** Cho KI, Sakuma I, Sohn IS, Jo SH, Koh KK. Inflammatory and metabolic mechanisms underlying the calcific aortic valve disease. *Atherosclerosis*. 2018;277:60–65.

**41.** Phadwal K, Vrahnas C, Ganley IG, MacRae VE. Mitochondrial dysfunction: cause or consequence of vascular calcification? *Front Cell Dev Biol*. 2021;9:611922.

**42.** Ballinger SW, Patterson C, Knight-Lozano CA, et al. Mitochondrial integrity and function in atherogenesis. *Circulation*. 2002;106:544–549.

**43.** Jeong SY, Seol DW. The role of mitochondria in apoptosis. *BMB Rep*. 2008;41:11–22.

**44.** Peoples JN, Saraf A, Ghazal N, Pham TT, Kwong JQ. Mitochondrial dysfunction and oxidative stress in heart disease. *Exp Mol Med*. 2019;51:1–13.

**45.** Rogers MA, Maldonado N, Hutcheson JD, et al. Dynamin-related protein 1 inhibition attenuates cardiovascular calcification in the presence of oxidative stress. *Circ Res*. 2017;121:220–233.

**46.** Hebert Chatelain E, Dupuy JW, Letellier T, Dachary-Prigent J. Functional impact of PTP1B-mediated Src regulation on oxidative phosphorylation in rat brain mitochondria. *Cell Mol Life Sci*. 2011;68:2603–2613.

**47.** Song Z, Ghochani M, McCaffery JM, Frey TG, Chan DC. Mitofusins and OPA1 mediate sequential steps in mitochondrial membrane fusion. *Mol Biol Cell*. 2009;20:3525–3532.

**48.** Anand R, Wai T, Baker MJ, et al. The i-AAA protease YME1L and OMA1 cleave OPA1 to balance mitochondrial fusion and fission. *J Cell Biol*. 2014;204:919–929.

**49.** Song Z, Chen H, Fiket M, Alexander C, Chan DC. OPA1 processing controls mitochondrial fusion and is regulated by mRNA splicing, membrane potential, and Yme1L. *J Cell Biol*. 2007;178:749–755.

**50.** Ge Y, Shi X, Boopathy S, McDonald J, Smith AW, Chao LH. Two forms of Opa1 cooperate to complete fusion of the mitochondrial inner-membrane. *Elife*. 2020;9:e50973. https://doi.org/10.7554/eLife.50973

**51.** Lee H, Smith SB, Yoon Y. The short variant of the mitochondrial dynamin OPA1 maintains mitochondrial energetics and cristae structure. *J Biol Chem*. 2017;292:7115–7130.

**52.** Lee H, Smith SB, Sheu SS, Yoon Y. The short variant of optic atrophy 1 (OPA1) improves cell survival under oxidative stress. *J Biol Chem*. 2020;295:6543–6560.

**KEY WORDS** calcific aortic valve disease, mitochondrial biogenesis, optic atrophy 1, protein tyrosine phosphatase 1B, valvular interstitial cells

**APPENDIX** For an expanded Methods section as well as supplemental figures and tables, please see the online version of this paper.